

Wen-Jong Chang,¹ Jyh-Fang Chen,² Hsing-Chuan Ho,³ and Yung-Fang Chiu⁴

In Situ Dynamic Model Test for Pile-Supported Wharf in Liquefied Sand

ABSTRACT: Pile-supported wharf is a general option in port design to provide lateral resistance and bearing capacity under both static and dynamic loadings. In situ large-scale physical modeling using surface wave generator was performed to study the dynamic soil-structure interactions in pile-supported wharves and to verify configuration of an in situ monitoring station. A wharf model consisting of two steel pipe piles welded on a steel slab was installed on a reconstituted underwater embankment. Due to screening of stress waves, the two piles are subjected to different loading conditions. Data reduction procedures were developed to analyze coupled shear strain-pore pressure generation behavior, pile responses, and soil-pile interaction characteristics. The results proved that the physical modeling can capture the interactions among the induced shear strain, generated excess pore pressure, and dynamic p - y behavior around piles. Preliminary results also show that evolutions of dynamic p - y curve with excess pore pressure variations should be included in soil-pile interaction modeling.

KEYWORDS: dynamic soil-structure interaction, pile-supported wharf, large-scale pile-liquefied soil modeling, soil liquefaction

Introduction

Soil liquefaction is the most widespread seismic damage to port and harbor facilities because native soils or hydraulic fills in ports are generally loose, saturated, and cohesiveless soils. Pile-supported wharves, consisting of a soil or rock underwater embankment, a rigid deck above the embankment, and piles connected to the deck, are common waterfront facilities providing lateral resistance and bearing capacity under both static and dynamic loadings. Pile-supported wharf failures in liquefied soils had been found at the port of Oakland during the 1989 Loma Prieta Earthquake (Werner et al. 1998), Takahama in Kobe during the 1995 Hyogo-ken Nambu Earthquake (Tokimatsu and Asaka 1998), and Andaman Island during the 2004 Sumatra Earthquake (Mondal and Rai 2008). Previous studies reveal that forces applied on wharf piles during seismic loading can be divided into inertial forces induced by vibrations of superstructure and kinematic forces from the relative deformations of surrounding soil. However, evaluations of inertial and kinematic effects in soil-pile systems involve highly complicated soil-pile-structure interaction mechanism, which remains a highly challenging issue in geotechnical earthquake engineering field (Cubrinovski et al. 2006; Rollins and Sparks 2002).

Techniques for analyzing soil-pile interaction in liquefiable sandy soils can be categorized into four branches: Pseudo-static analyses (e.g., Rollins et al. (2005)), dynamic numerical simulations (e.g., Boulanger et al. (1999) and Klar and Frydman (2002)), laboratory physical modeling (e.g., Brandenberg et al. (2005) and Takahashi and Takemura (2005)), and in situ dynamic testing (e.g.,

Rollins et al. (2005) and Kamijo et al. (2004)). In pseudo-static analyses, simplified p - y concept (Wang and Reese 1998), which defined the relationship of horizontal subgrade reaction with the relative displacement between the pile and surrounding soil, was generally used to represent the soil-pile interaction and a p -multiplier was used to account for the reduction of p - y curve in liquefied soil (Rollins et al. 2005). The major limitations of the pseudo-static analysis are case dependent and over simplification. In numerical simulations, different forms of beam on Winkler foundations (BWF) are used to link the response between the pile and the surrounding soil. Boulanger et al. (1999) proposed the beam on nonlinear Winkler foundation (BNWF) model, which uses a serial combination of gap, plastic, and elastic springs to simulate the nonlinear dynamic response of soil-pile interaction. The complexity of the mechanism and knowledge involved makes these numerical simulations require rigorous verifications. To improve the applicability of pseudo-static approaches and verify numerical results, large-scale physical modeling and long waiting field monitoring stations are required.

Many insights of soil-pile interaction behaviors come from observations and interpretations of laboratory physical modeling. Techniques used in this category include 1 g shaking table tests (Tokimatsu and Suzuki 2004) and centrifuge tests (Brandenberg et al. 2005). However, due to the complexity of in situ soil stratum, nonlinear soil responses, and disturbance from pile installation, in situ dynamic soil-pile interaction testing is preferred and sometimes the only option in evaluating the site specific liquefaction responses of pile-support wharves. Rollins et al. (2005) and Kamijo et al. (2004) used controlled blasting to induce soil liquefaction in the field and observed the soil and pile responses. Due to the damage from blasting, this type of technique is not suitable for active facilities. Alternatively, the installation of a long waiting instrumentation on active wharves for future seismic events and the development of testing techniques that can directly measure the soil-pile-structure interactions under controlled loading are warranted.

This paper presents a pilot test which implemented the in situ dynamic liquefaction test proposed by Rathje et al. (2005) on a wharf model in liquefiable soil. The test aimed to (1) verify the con-

Manuscript received March 19, 2009; accepted for publication February 11, 2010; published online March 2010.

¹Assistant Professor, Dept. of Civil Engineering, National Cheng Kung Univ., Tainan 70101, Taiwan, e-mail: wjchang@mail.ncku.edu.tw

²Associate Researcher, Harbor and Marine Technology Center, Institute of Transportation, Wuchi, Taichung 435, Taiwan.

³Research Engineer, Geotechnical Engineering Research Center, Sinotech Engineering Consultants, Inc., Taipei 11071, Taiwan.

⁴Director, Harbor and Marine Technology Center, Institute of Transportation, Wuchi, Taichung 435, Taiwan.

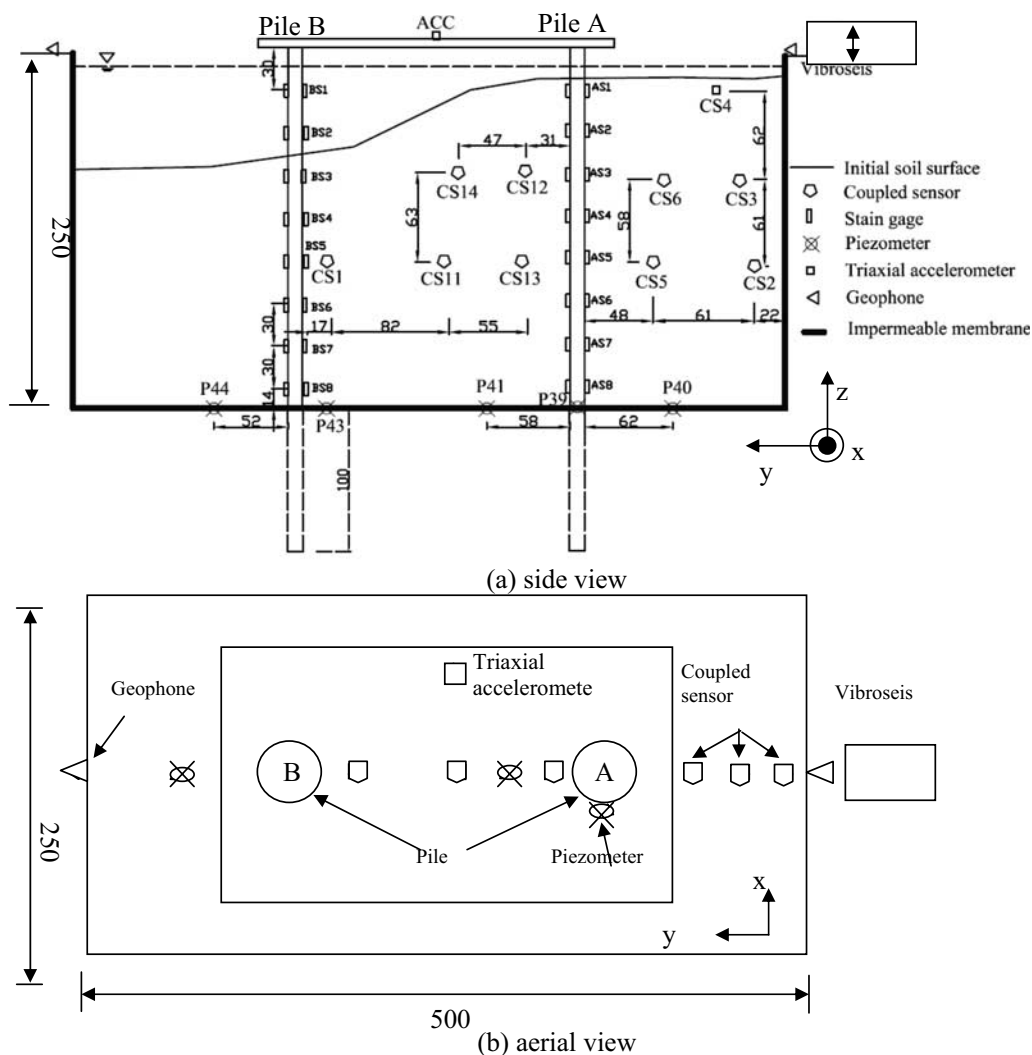


FIG. 1—Layout of wharf model test (unit: centimetre).

figuration of in situ seismic monitoring stations on active wharf facilities, (2) develop a technique for integrity check of the in situ instrumentation system, and (3) perform a seismic soil-structure interaction study on pile-supported wharves. A vibroseis truck, which is a mobile servo-hydraulic shaker mounted on a transport vehicle, was used to generate surface waves propagating laterally to a large-scale wharf model. The dynamic source produced a uniform stress profile laterally applied on middle section of the pile, which is useful in studying the BNWF behaviors around piles. Instrumentation was configured to measure dynamic soil motions, pore pressure variations, and pile responses. A data reduction procedure was developed to extract nonlinear soil properties, coupled shear strain-pore pressure response, pile responses, and soil-pile interactions.

Testing Methodology

Analyses of pile-supported wharves on liquefiable soil require studying of dynamic behavior of pile system, nonlinear soil responses with pore pressure generation, and soil-pile-superstructure interactions. The in situ model test involves dynamically loading wharf model in the field while simultaneously measuring the soil and wharf model responses. To account for different loading modes

between the real earthquake excitations due to upward propagating shear waves and the laterally propagating surface waves in proposed test, soil responses are analyzed on shear strain basis instead of soil motion quantities such as acceleration or velocity. Configured instrumentation was used to evaluate induced shear strains, pore pressure variations, wharf responses, and soil-pile interactions.

Testing Layout and Dynamic Source

Testing components of the dynamic wharf model test include a surface dynamic loading system, a wharf model on liquefiable underwater embankment, and configured instrumentation. Testing layout and configuration of the in situ wharf modeling are shown in Figs. 1 and 2. The testing site is a reclaimed land in Taichung Harbor, Taiwan. The native soil profile characterized by boring and seismic survey is tabulated in Table 1. The top 4 m of field soil is backfilled crust with Unified Soil Classification System (USCS) classification of silty sand (SM), and the average shear wave velocity of this layer is 200 m/s. The soil below the crust is hydraulic filled silty sand classified as SM with shear wave velocity from 200 to 310 m/s. The ground water table varies with tides and within depths of 3.5–5.0 m.

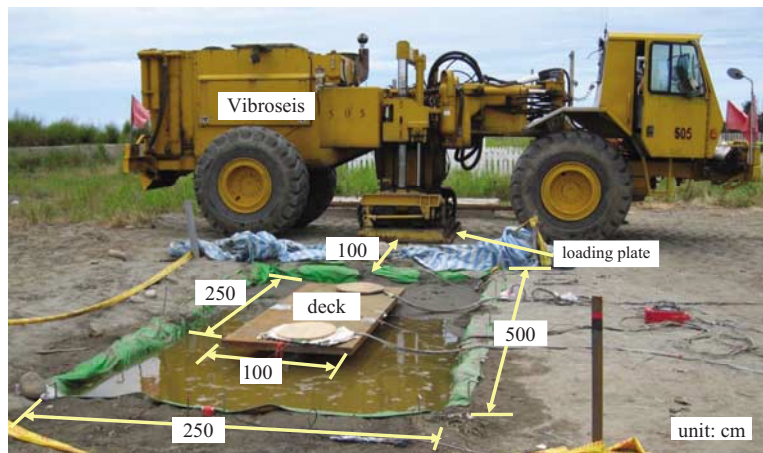


FIG. 2—Vibroseis truck and setup of wharf model test.

The surface dynamic loading source consists of a vibroseis truck and a rectangular loading plate. The vibroseis truck served as a vertical vibration source that dynamically loaded the rectangular steel plate on the ground surface. The loading plate is placed 1 m from the tested model and lined up on the center line of the model for symmetric consideration. The symmetric alignment between the dynamic source and the model reduced the three-dimensional conditions to a two-dimensional (2D) plane wave configuration. This dynamic loading system generated surface waves that propagated laterally through the wharf model, cyclically shearing the model soil, and continuously applying forces on piles and the deck plate. The vibroseis truck (Fig. 2) used in this test can generate sinusoidal waves with a frequency range of 7–100 Hz, maximum amplitude of 225 kN, and duration of up to 30 s. A similar system used by Rathje et al. (2005) had proven that the generated surface waves are capable of inducing shear strain amplitude greater than the general threshold shear strain level ($\sim 10^{-2}$ %) and generating significant excess pore pressure.

Preparation of Wharf Model

A model wharf consisting of two steel pipe piles with pile heads welded on a steel plate was installed on a reconstituted underwater embankment to represent a pile-supported wharf on liquefiable soil. The dimensions of deck plate are $250 \times 100 \times 1$ cm³ with respect to length, width, and thickness. Each steel pipe pile is 350 cm long with a 20 cm outer diameter and 0.5 cm thickness. The bottom 100 cm of piles was pushed into the native soil statically after trench excavation, and the remaining 250 cm was buried by the reconstituted soil. After the driving of piles, the deck plate was welded on top of piles as rigid connections and the horizontal distance between the two piles was 190 cm from center to center.

To produce uniform saturated soil stratum, the reconstituted underwater embankment was prepared by water sedimentation. The reconstituted soil was divided into seabed, underwater slope, and

level backfill. The seabed and the level backfill were constructed from two ends of the trench, and the underwater slope was formed in the natural rest angle of soil. A test trench with dimensions of $5.0 \times 2.5 \times 2.5$ m³ with respect to length, width, and depth, respectively, was excavated. Because native ground water table is below 3 m, a thin impermeable membrane was placed on the excavated surface to prevent water leakage from the trench and maintain the saturation of the reconstituted soil. Soil borrowed from the nearby beach was used to prepare the underwater embankment. The borrowed soil is a non-plastic, clean, and fine sand classified as SM soil in USCS classification with a specific gravity of 2.66. Post-test borings confirmed that the spatial variations of void ratio and unit weight were small, indicating that the reconstituted soil was quite uniform. The reconstituted soil has an initial void ratio of 0.94 and saturated unit weight of 18.1 kN/m³. Bender element tests on reconstituted specimens showed that the shear wave velocity at 1.25 m deep was 80 m/s, and the value was checked by the travel time of wave propagation in the level backfill. This shear wave velocity corresponds to a normalized shear wave velocity (V_{s1}) of 156 m/s, which will liquefy under small cyclic stress ratio (~ 0.1) for earthquakes of magnitude of 7.5.

Instrumentation

To simultaneously monitor soil motions and pore pressure variations, the “coupled sensor” was fabricated by integrating a triaxial low frequency accelerometer and a miniature pore pressure transducer in an cylindrical acrylic case of a size of 55 mm in diameter and 78 mm in length (without cone). A detachable cone was provided for field installation and was not attached in this configuration. Figure 3 shows details of the coupled sensor. A triaxial capacitive accelerometer was used for measuring the local ground accelerations in the vertical and two orthogonally horizontal directions. The compact size (a 28 mm cube) of the accelerometer significantly reduces the size of the couple sensor, and the low frequency feature (dc to 100 Hz in 95 % accuracy) makes it fit for the frequency content of real earthquakes. To reduce the vibration influence from the extension cable, the wire connections within the acrylic case are connected with a 30 cm long flexible multi-connection signal cable. A shield, five-paired polyvinyl-chloride insulated cable, which is more resistant to erosion, tension, and electrical noises, is connected to the flexible cable and extended to connect with data acquisition systems.

TABLE 1—Soil profile of testing site within 20 m deep.

| Layer | Depth (m) | USCS Classification | V_s (m/s) |
|---------|-----------|---------------------|-------------|
| Crust | 0–4.5 | ML | 200 |
| Layer 1 | 4.5–11.0 | SM | 200 |
| Layer 2 | 11.0–20.0 | SM | 220–310 |

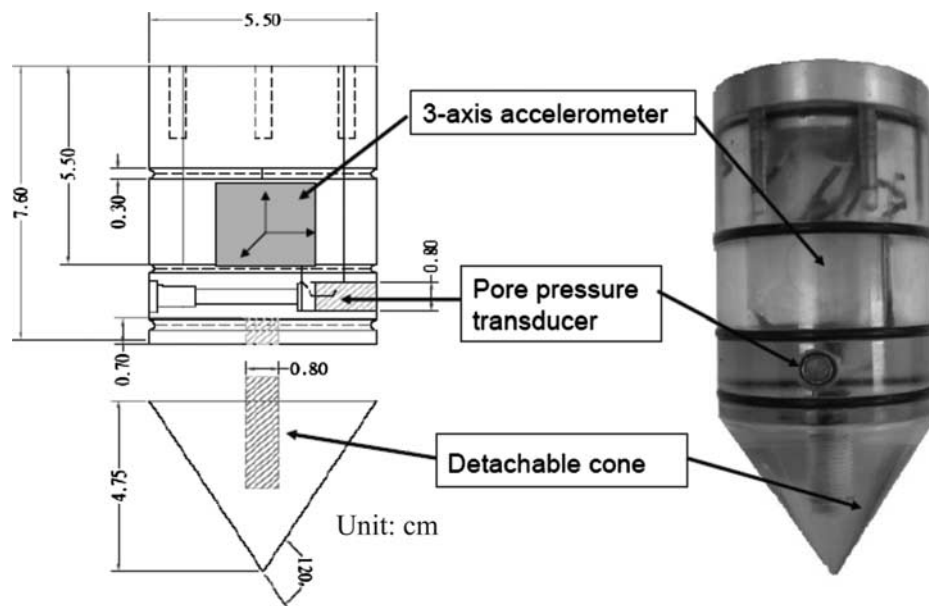


FIG. 3—Detail of coupled sensor.

Eight coupled sensors were deployed, as shown in Fig. 1, to form two 0.6×0.6 m² arrays on the vertical plane along the center line of the trench. For each coupled sensor, the three accelerometer axes were oriented to the three coordinate directions (x , y , and z in Fig. 1) of the model. One array was deployed on the level backfill, and the other was deployed behind pile A. These coupled sensors were used to calculate strains within the array and evaluate spatial variations of soil motion and pore pressure. Other embedded sensors include one coupled sensor placed near the top of the level backfill, another one in front of Pile B, and five piezometers (P39, 40, 41, 43, and 44) at the bottom of the test pit.

Pile responses were monitored by strain gage pairs glued on opposite sides of a pile with 30 cm vertical interval to measure the induced bending strain profiles. The advantages of this type of strain gage layout include temperature compensation, cancelation of thermal effect of lead wires, removal of axial strain, and double magnitude of output voltages. The calibration of strain gage pairs using simple beam setup with a point load at the center of the beam shows that the strain gage pair is valid for bending strain of less than 3%. Using an elastic beam theorem with proper end conditions, profiles of moment distribution, lateral displacement, and subgrade reaction on piles can be evaluated. Deck plate motion was measured by a triaxial accelerometer and used to verify the evaluated lateral displacements of piles.

All the embedded sensors were installed before the water sedimentation process. Piezometers and coupled sensors were fixed at the designated locations with proper orientations by fishing lines after excavation. All fishing lines were cut prior to shaking test to make sensors move with the soil. A customized stand-alone dynamic data acquisition system was used for these sensors. This data acquisition system provides (1) high sampling rate, (2) different durations for vibration sensors and pore pressure transducers, and (3) flexibility for field implementations. In the performed tests, data acquired from accelerometers and piezometers were collected at a sampling rate of 1000 Hz for better resolution in wave velocity determination by travel time interval and smoother integration for soil displacement and velocity calculations. Piezometer data were continuously recorded after shaking to capture the dissipation process

of the excess pore pressures. Down-sampling technique was adopted in data processing to reduce data points of pore pressure time histories.

Testing Procedure

A total of 15 test events was conducted, and details of the testing program are tabulated in Table 2. Three test series were conducted to study the effects of loading amplitude, frequency, and soil properties on soil-pile interactions. In test series A, the loading amplitude increased gradually with the largest loading amplitude in event 8, and only part of the reconstituted soil was liquefied. Test series B was conducted to study the soil-pile interaction in liquefied soil. Test series C was designed to investigate the effects of loading frequency on dense sand. Several small amplitude tests were performed for system check and wave velocity measurements. After each test event, surface survey was conducted to monitor the surface variations and induced settlements.

Data Analysis

Data collected from the embedded instrumentation include histories of particle motion, pore pressure, pile bending strain, and deck acceleration. These data were processed and analyzed to evaluate the temporal and spatial variations of shear strain and excess pore pressure induced in the embankment, horizontal pile deformations, subgrade reactions, and nonlinear soil-pile interactions. The data reduction procedure is shown in Fig. 4, and details are described below.

Shear Strain Evaluation

To be comparable with real seismic excitations mainly due to upward propagating shear waves, soil responses were represented in terms of induced shear strain instead of soil particle motion quantities. The testing configuration was setup in a plane wave condi-

TABLE 2—List of testing program.

| Series | Event | Frequency (Hz) | Load | | Purposes |
|--------|-------|----------------|----------------|--------------|---|
| | | | Amplitude (kN) | Duration (s) | |
| A | 0 | 10 | 11.3 | 5 | System check |
| | 1 | 10 | 22.5 | 5 | (1) Effects of amplitude, (2) pore pressure generation behavior, and (3) spatial variations of strain |
| | 2 | 10 | 33.8 | 5 | |
| | 3 | 10 | 45 | 5 | |
| | 4 | 10 | 56.3 | 5 | |
| | 5 | 10 | 67.5 | 5 | |
| | 6 | 10 | 78.8 | 10 | |
| | 7 | 10 | 112.5 | 15 | |
| 8 | 10 | 202.5 | 20 | | |
| B | 9 | 15 | 202.5 | 30 | Liquefied test |
| | 10 | 10 | 22.5 | 5 | Post-liquefaction system check |
| C | 11 | 10 | 22.5 | 5 | System check |
| | 12 | 10 | 22.5 | 5 | (1) Effects of frequency and (2) liquefaction in dense sand |
| | 13 | 10 | 202.5 | 30 | |
| | 14 | 15 | 202.5 | 30 | |
| | 15 | 20 | 202.5 | 30 | |

tion, and only the shear strains on the vertical plane of the center line needed be considered. Validations of the plane wave condition were confirmed from small soil motions in the direction normal to the vertical plane (*x*-direction in Fig. 1(a)).

To calculate the induced shear strains under the complicated wave field, the 2D displacement-based method (denoted as 2DBM) described in the work of Rathje et al. (2005) was implemented. The instrumentation array formed by four coupled sensors is considered as a four-node element with two degrees of freedoms (vertical and horizontal) per node. The vertical and horizontal directions are parallel to the particle motion direction (i.e., *z*- or *y*-direction), respectively. Taking the instrument array within the level backfill (CS2, 5, 6, and 3) as an example and assuming that the element size in Fig. 1(a) is approximately $2a$ in both *y*- (horizontal) and *z*- (vertical) directions and the origin ($y=0, z=0$) of the element is at the center of the array, the coordinates of the four coupled sensors are $(-a, -a)$, $(a, -a)$, (a, a) , and $(-a, a)$ for CS2, CS5, CS6, and CS3, respectively. On *yz*-plane, the shear strain at any point within the array with coordinates (y, z) , γ_{yz} , is evaluated by

$$\begin{aligned} \gamma_{yz}(y,z) = & \frac{1}{4a} \left[-u_{y2} \left(1 - \frac{y}{a} \right) - u_{z2} \left(1 - \frac{z}{a} \right) - u_{y5} \left(1 + \frac{y}{a} \right) \right. \\ & + u_{z5} \left(1 - \frac{z}{a} \right) + u_{y6} \left(1 + \frac{y}{a} \right) + u_{z6} \left(1 + \frac{z}{a} \right) + u_{y3} \left(1 - \frac{y}{a} \right) \\ & \left. - u_{z3} \left(1 + \frac{z}{a} \right) \right] \end{aligned} \quad (1)$$

where:

u_{ij} = displacement in the *i* direction (*i* = *y* or *z*) at node *j* (*j* = CS2, 5, 6, and 3).

The nodal displacements are computed by double integration on the vertical and horizontal acceleration histories with baseline corrections applied to remove the drifts by noises. To evaluate the coupled shear strain–pore pressure response at locations of coupled sensors, shear strains at the locations of coupled sensors needed to be evaluated. For example, the shear strain at CS5 (i.e., $y=a, z=-a$) is evaluated by

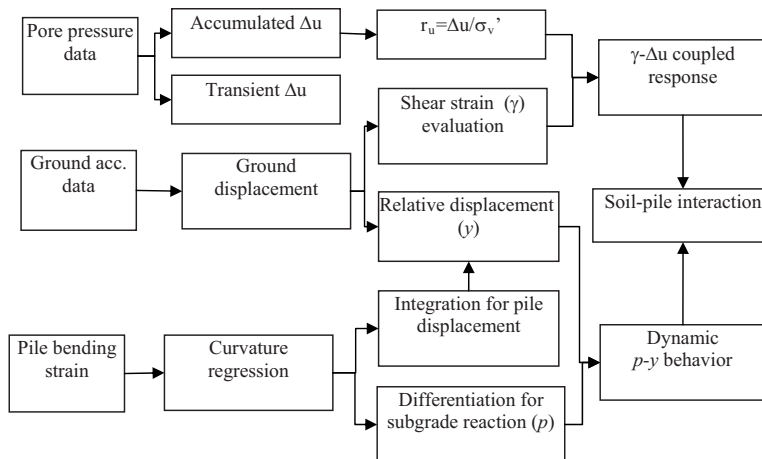


FIG. 4—Data reduction procedure.

$$\gamma_{yz}(y=a, z=-a) = \frac{1}{2a}[-u_{y5} + u_{z5} - u_{z2} + u_{y6}] \quad (2)$$

where:

$a=30$ cm with displacement unit of centimetre.

Excess Pore Pressure Ratio

The recorded pore pressures contained three components: (a) The hydrostatic pore pressure of the ground water table, (b) the transient excess pore pressure oscillating with the dynamic loading, and (c) the accumulated excess pore pressure (Δu) representing the net outcome between the accumulation and dissipation of the excess pore pressure. To focus on excess pore pressures, hydrostatic pore pressures were subtracted from the records. To highlight and analyze the transient and accumulated excess pore pressures separately, band-passing and low-passing filters are used, respectively. To calculate the excess pore pressure ratio ($r_u = \Delta u / \sigma'_{v0}$), defined as the accumulated excess pore pressure (Δu) normalized to the initial vertical effective stress (σ'_{v0}), the initial vertical effective stress was inferred from the submerged unit weight of soil ($\gamma' = \gamma_{\text{sat}} - \gamma_w = 8.3$ kN/m³) and the depth of sensor. Initial liquefaction is defined as the state that the accumulated excess pore pressure reaches the initial vertical effective stress or r_u is a unity. Combining the computed shear strain at the location of pore pressure measurement, the coupled response of the shear strain and the excess pore pressure can be evaluated.

Pile Behavior and Soil-Pile Interaction

On a BWF framework, soil-pile interaction at a specific depth is described as

$$EI \frac{\partial^4 y}{\partial z^4} = kD(y_s - y) \quad (3)$$

where:

E and I =Young's modulus and moment inertia of the pile, respectively,

y =lateral deflection of pile,

y_s =horizontal displacement of soil,

k =modulus of horizontal subgrade reaction, and

D =pile diameter.

For the steel model piles, $E=2.1 \times 10^{11}$ N/m², $I=1.7 \times 10^{-5}$ m⁴, and $D=0.2$ m. Assuming that the beam behaves linearly and the cross section of the pile is uniform, the curvature (κ) of pile, bending strain (ε), and lateral deflection (y) at a depth of z is related by

$$\kappa(z, t) = \frac{[\varepsilon_n(z, t) - \varepsilon_s(z, t)]}{D} = \frac{\partial^2 y(z, t)}{\partial z^2} \quad (4)$$

where:

ε_n and ε_s =bending strain on opposite side with distance of D in the direction normal to neutral plane.

For strain gage pairs on opposite sides, $\varepsilon_s(z)$ is equal to $-\varepsilon_n(z)$, and D is constant. With specified end conditions, the horizontal displacement of pile can be evaluated by

$$y(z, t) = \int \int \kappa(z, t) dz dz \quad (5)$$

The horizontal displacement of soil is evaluated from numerical double integration of acceleration data. The relative displacements between the pile and soil were evaluated accordingly.

The bending moment on the pile is

$$M(z, t) = EI \frac{\partial^2 y(z, t)}{\partial z^2} = EI \kappa(z, t) \quad (6)$$

The net distributed horizontal stress (p) per unit length on the pile is

$$q(z, t) = EI \frac{\partial^4 y(z, t)}{\partial z^4} = EI \frac{\partial^2 \kappa(z, t)}{\partial z^2} \quad (7)$$

The subgrade reaction of soil on pile, p , expressed as the net horizontal force of unit length, is calculated from

$$p(z, t) = q(z, t) = kD \quad (8)$$

Combine the subgrade reaction from Eq 7 and relative displacement between the pile and surrounding soil and, the p - y behavior was established.

The above expressions are based on continuous functions; however, the measured data are discrete. Curve fitting functions with existence of second derivatives have been used to interpret lateral response of piles subjected to lateral loading. The most common fitting techniques for pile tests are polynomial functions (Dunnivant and O'Neill 1989) and cubic spline interpretation (Dou and Byrne 1996). The advantages of using cubic spline interpolation include (1) passing every measured point smoothly, (2) avoidance of error accumulation with order of polynomials, (3) being applicable to limited data points, and (4) simplicity (Nakamura 1995). The cubic spline interpolation is used in this study with specified boundary conditions at both pile ends. Because the top of the pile is welded on the steel deck and the deck move horizontally, zero curvature at the pile top is assumed. Although the pile is 3.5 m long, only the portion within the reconstituted soil (2.5 m) was measured, and the bottom 1.0 m was penetrated in the native soil, which was neither liquefied nor subjected to large stiffness reduction due to small shear strain level. As a result, a fixed portion of piles within the native soil is assumed. The curvature at the bottom of the test pit is linearly extrapolated from the lowest measuring point (0.14 m from bottom). These two end conditions were used in the cubic spline interpolation of pile curvature.

The fitted curvature curves were doubly integrated to compute the distribution of lateral displacement and differentiated twice to estimate the profile of subgrade reaction in every time step. In numerical calculations, low frequency noise increases the errors of integration and high frequency noise increases the errors of differentiation. To minimize the effects of noise on numerical calculations, band-passing filter, which retained components with 0.5–1.5 times of loading frequency, was applied on bending strain histories before numerical calculations. Verifications of end condition assumptions and filtering effects were conducted by comparing the pile head displacement amplitudes with the measured relative deck displacement amplitudes estimated from double integration of the deck acceleration subtracting the bottom displacement, and the results are shown in Fig. 5. The average pile head amplitudes of the two piles, which take into account of the deformation of deck plate, agree well with the relative deck displacement amplitudes, indicating that the procedure for bending strain processing is adequate for

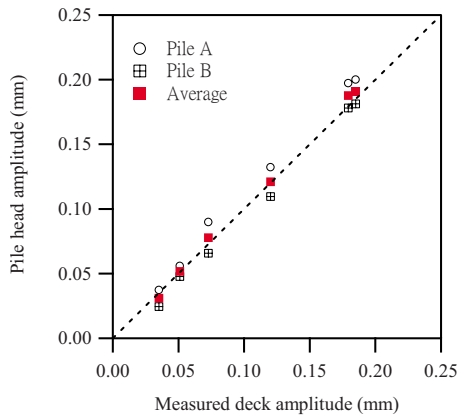


FIG. 5—Comparison of deck displacement amplitude.

displacement evaluation. The validation of subgrade reaction evaluation is more complicated. However, qualitative agreements in the observed soil-pile interactions provide certain degree of confidence on the evaluated results.

Typical Testing Results

As indicated in Table 2, event 9 is the first test where liquefaction occurred in the entire embankment; therefore, results of event 9 are presented to show the wharf responses in liquefied sand. Results of the coupled shear strain-pore pressure response and the temporal and spatial variations of excess pore pressure are presented to demonstrate the liquefaction process. Dynamic *p-y* behavior is evaluated from piles and adjacent soil responses to represent the dynamic soil-pile interactions.

Pore Pressure Variations

The accumulated excess pore pressure histories of event 9, processed by low-passing 1 Hz, are shown in Fig. 6 along with the time of initial liquefaction. Variations of excess pore pressure at level backfill, slope, and bottom of test pit are presented in group to demonstrate the liquefaction process of the embankment. The initial liquefaction was first observed at CS5 (Fig. 6(a)) and CS12 (Fig. 6(b)), where relatively large accelerations were observed as shown in Fig. 7. After the initial liquefaction at CS5 and CS12, initial liquefaction was observed at the bottom of the embankment. The location of CS4 (0.4 m deep) was not liquefied due to the smaller induced shear strain and faster dissipation.

Time histories of excess pore pressures at the bottom of the test pit are shown in Fig. 6(c), which indicated that the initial liquefaction was first occurred near the piles and quickly extended laterally. The same trend was observed at the depth of 1.6 m, where initial liquefaction was observed in the sequence of CS5, CS13, and CS1. The temporal variations of liquefaction process indicated that the existence of pile affected the pore pressure accumulation and the rate of pore pressure accumulation decreases as the distance to the pile increases. Detail mechanism is better explained from the coupled strain-pore pressure response and pile behavior, which are presented in next section.

Soil Coupled Response

Spatial variations of soil acceleration histories in the level backfill and slope are shown in Fig. 7(a) and 7(b), respectively. In Fig. 7 all

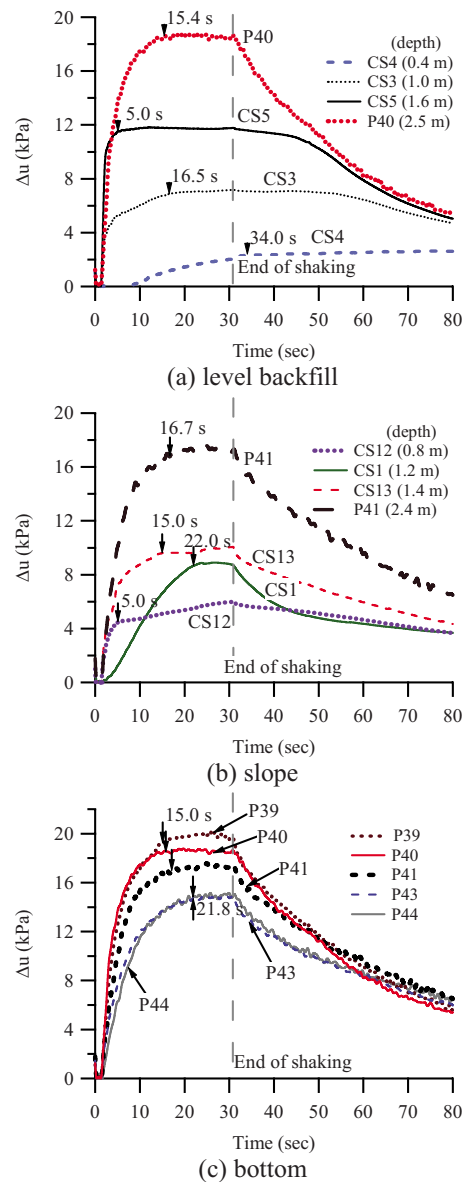


FIG. 6—Variation of accumulated excess pore pressure (low-passing 1 Hz) in liquefied case (event 9).

the data are processed with band-passing filter of frequency between 7.5 and 22.5 Hz. The vertical and horizontal motion components within level backfill generally agree with the wave characteristics of Rayleigh waves, including retrograde elliptical particle traces, higher amplitude in vertical component except near surface, and varied vertical amplitude with maximum value at the depth of 1/3 wavelength (Woods 1968). However, the motion sensors at the slope recorded different motion patterns. The horizontal component of soil behind pile A is very small except CS14, where the location was close to the sloping surface and the reflected waves from the sloping surface were recorded. The significant reduction in both horizontal and vertical motions behind the pile is the outcome of screening effects of stress waves due to the pile, and the shear strain is significantly reduced, as shown in Fig. 8.

The induced shear strains at locations of CS5 and CS13 calculated by 2DBM are plotted along with the corresponding excess pore pressures in Fig. 8(a) and 8(b), respectively, to show the coupled shear strain-pore pressure responses ahead and behind pile

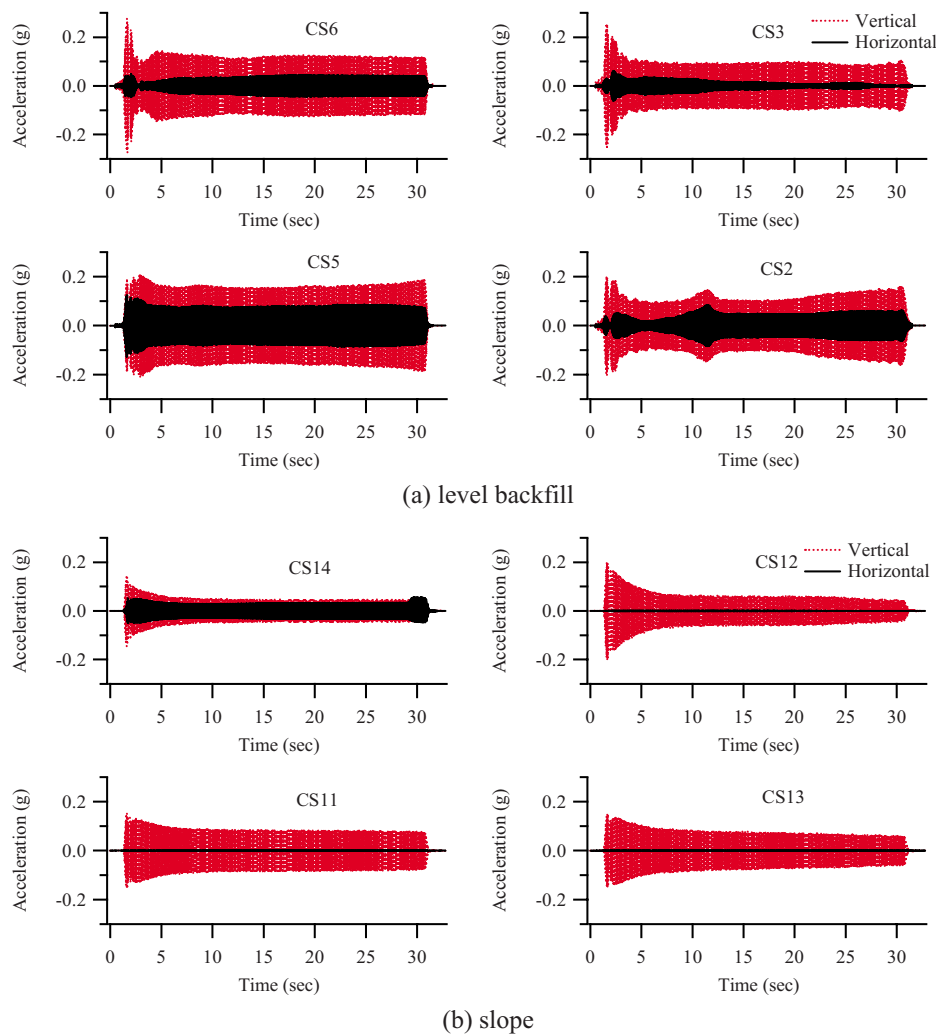


FIG. 7—Acceleration records for event 9 (band-passing 7.5–22.5 Hz).

A. The coupled shear strain–pore pressure response at CS5 agreed with a typical response of saturated sand in level free field in terms of deformation mode and pore pressure generation pattern. In the backfill, the induced shear strain is contributed by both vertical and horizontal nodal displacements, and the pore pressure generation can be divided into four phases, as described by Chang (2002).

The coupled response behind pile A showed significant reductions in shear strain due to screening of stress waves (Fig. 8(b)). Although the amplitude of shear strain at CS13 is at the margin of threshold shear strain, the generated excess pore pressure still reached initial liquefaction state later. Similarity among the pore pressure histories at the bottom and the nearby coupled sensor (CS13 versus P41 and CS1 versus P43) indicates that the excess pore pressures behind pile A were not only solely generated from induced shear strains but also affected by the hydraulic gradients among surrounding soils.

Dynamic Soil–Pile Interaction

Time histories of bending strains and lateral displacements of pile A in event 9 are shown in Fig. 9, respectively. The distribution of bending strains also represents the profile of bending moment of the pile according to Eqs 3 and 5. Profiles of bending strain, lateral

deflection, and subgrade load of pile A during the largest response cycle in event 9 are shown in Fig. 10(a). The maximum bending strain/moment was observed at the middle of the pile (from 90 to 150 cm deep), then gradually decreased as the depth decreased. The displacement profiles show that the pile vibrated in the fundamental mode with fixed end near the bottom of the trench and zero curvature at the top. The subgrade load distributions shown in Fig. 10(a) indicate that a uniform subgrade pressure was applied at the middle section of the pile. The uniform lateral pressure section provides a better controlled condition in back-calculating the p - y response. Nevertheless, the results demonstrate that pile A was mainly subjected to kinematic forces from surrounding soil due to stress wave propagation.

However, responses of pile B at the same time steps are different, although the pile head displacements are close, as shown in Fig. 10(b). The response profiles of pile B indicate that pile B was under a pushover condition with forced displacement on top in which the inertial forces are more dominating. The nonzero subgrade load above the ground surface is a numerical error due to limited measurement points in cases of a point load on pile head. The cause of the different loading condition of Pile B is the outcome of screening effects and rigid connections of piles on the deck plate. Although the current configuration induced two different

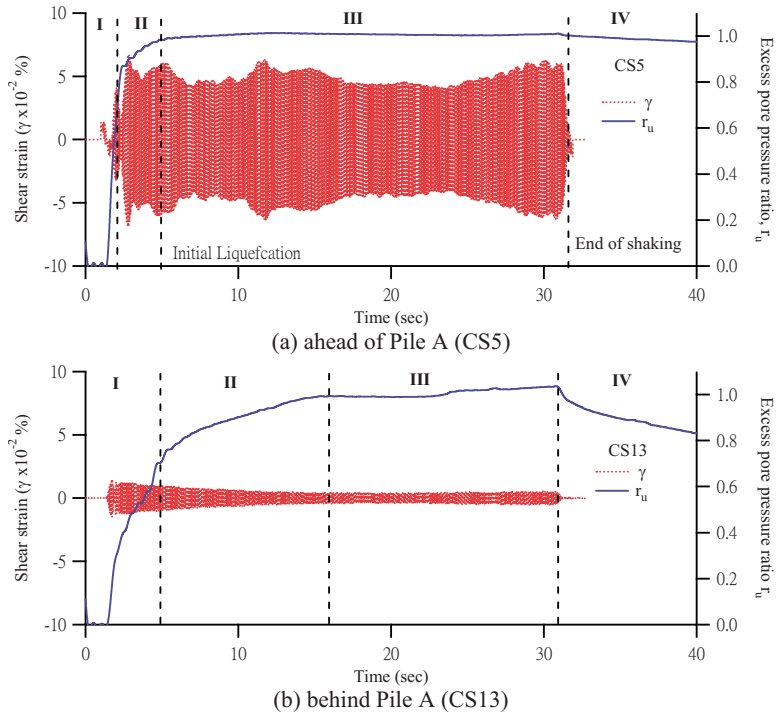


FIG. 8—Coupled shear strain-pore pressure response in liquefied case (event 9).

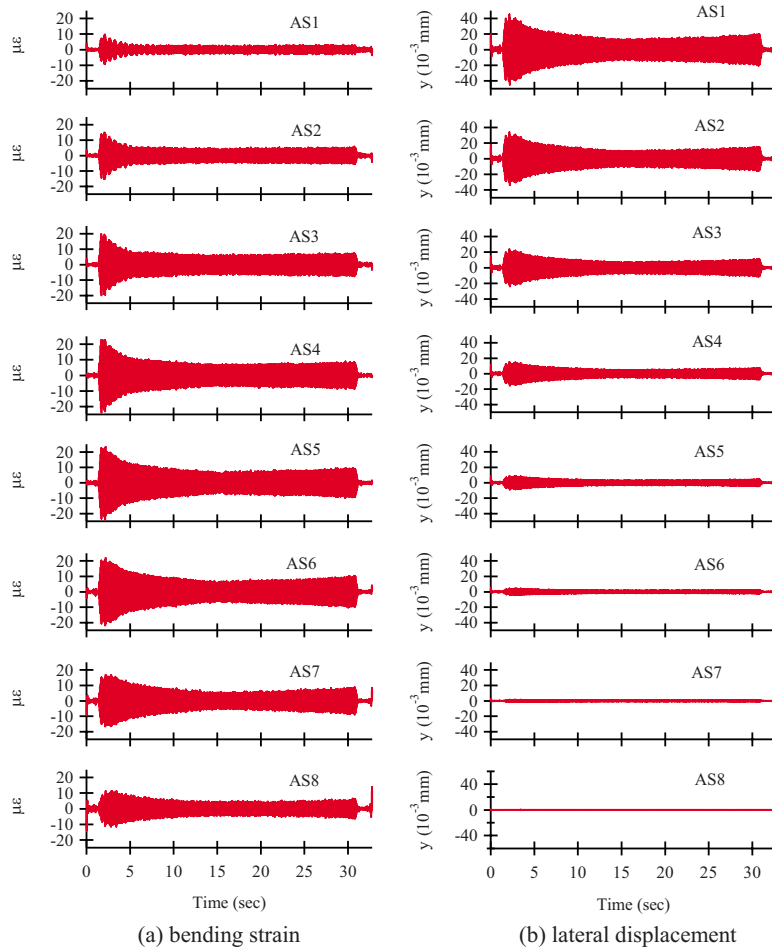


FIG. 9—Response histories of pile A at sensor locations in event 9 (filtered data).

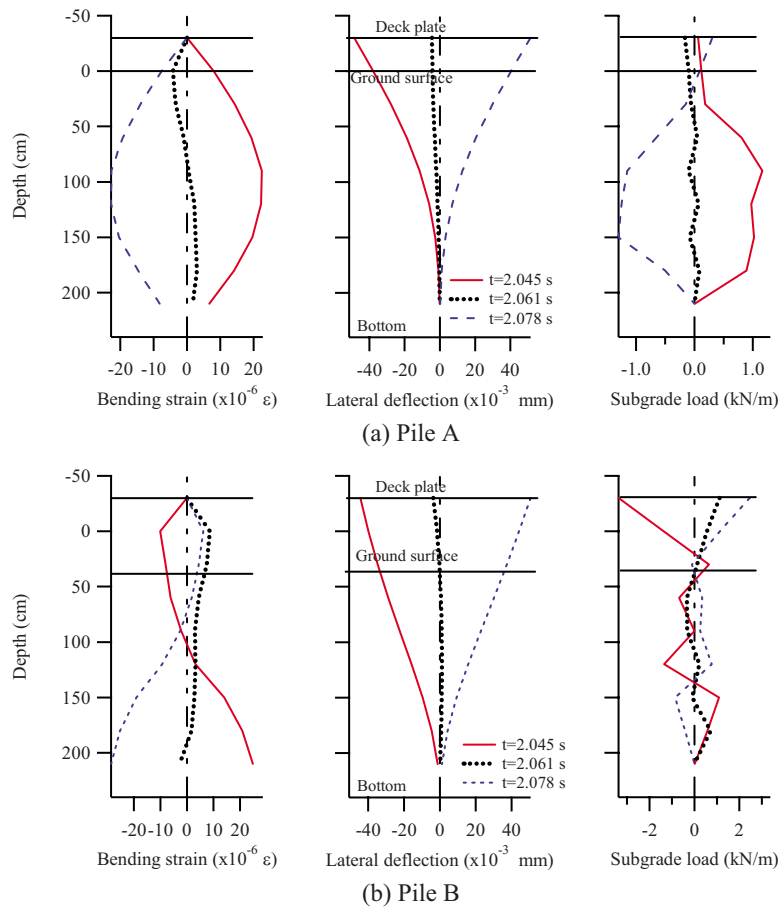


FIG. 10—Response profiles of piles in event 9.

loading mechanisms of piles on same deck plate, it provides a testing technique that can study the two loading conditions in one test and could represent pile groups subjected to inclined waves.

Figure 11 shows the dynamic p - y curves of Pile A at different depths with three excess pore pressure ratios calculated from adjacent pore pressure measurements in level backfill (P39, P40, CS5, and CS3). The hysteretic curve of p - y response is similar to the BNWF model proposed by Boulanger et al. (1999). These figures demonstrate that the dynamic p - y curves were significantly affected by the generated excess pore pressure ratio of surrounding soils. For clear demonstration, the evolution of p - y curves with pore pressure ratio variation at the depth of 1.5 m are combined and shown in Fig. 12. At low r_u , the p - y curves behaved almost linearly due to relatively constant soil stiffness and stress amplitude. As the excess pore pressure ratio increased, the secant modulus of the hysteretic loops decreased, and the areas of the loops increased, indicating that subgrade pressures have reduced and damping effects have increased. The evolution of dynamic p - y is the outcome of reduced soil stiffness and change of soil impedance.

Combining the results of coupled soil responses and dynamic p - y behavior revealed that soil stiffness variations due to pore pressure generation and induced strain level should be considered in dynamic p - y framework for liquefied sand. Also, the preliminary results proved that the testing configuration can capture major characteristics of pile-support wharf under kinematic and inertial excitations.

Discussion

The performed test used surface wave generator to cyclically load a model wharf and trigger liquefaction of submersed soil. Due to the difference in loading mode, concerns of applying the results to real seismic loadings rise. To make the testing results comparable to real seismic excitations from upward propagating shear waves, a new analyzing framework has been adopted. First, the soil responses are processed and presented in terms of induced shear strains instead of the ground accelerations. Shear strains represent the deformation of soil and dynamic soil properties, and induced excess pore pressures are shear strain level dependent. Because excess pore pressure generation is independent of deformation plane, therefore the loading modes will not significantly affect the pore pressure generation. As a result, using induced shear strains to represent soil disturbance is more direct and rigorous in mechanics than ground accelerations.

Second, although the surface waves applied both vertical and horizontal forces on a pile, only the horizontal component will induce bending strain, and the vertical component will induce only axial strain for small bending strain condition. As a result, analysis procedures for pile p - y responses are the same for both surface and shear wave loadings. Third, different loading mechanisms on the two piles due to screening effect had been identified, and kinematic and inertial forces are analyzed separately. Considering the framework of shear evaluation, separation of kinematic and inertial loadings, and small deformation of pile system, the proposed testing are

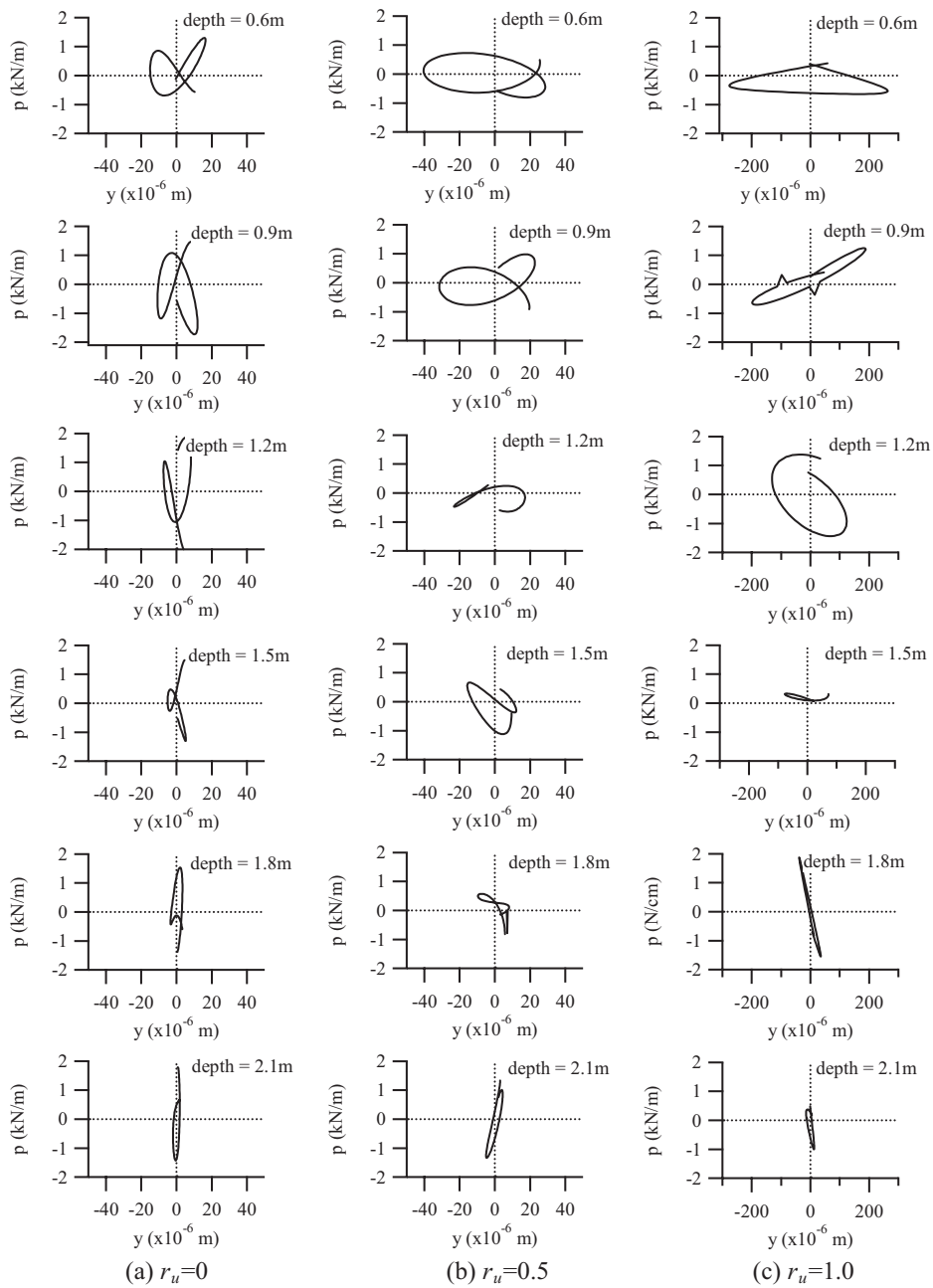


FIG. 11—Dynamic p - y response of pile A at different r_u .

generally comparable with real seismic excitations and shaking table tests.

Reductions in both acceleration amplitudes (Fig. 7) and induced shear strains (Fig. 8) behind pile A indicate that significant screening effects existed in current configuration. The reduction could be attributed to screening effect from pile A, stress wave barrier due to liquefied zone, and geometric damping. The geometric damping is small due to the small ratio of the distance between two evaluated points and the wavelength (~ 13 m). The amplitude reduction due to ahead liquefied zone should be observed after the initial liquefaction within level backfill. However, significant amplitude reduction had observed from the beginning of the loading. As a result, the screening effects should be mainly from the installation of pile A. It should be noted that the screening effect is less significant in real seismic excitations because level bedrocks and upward propagating

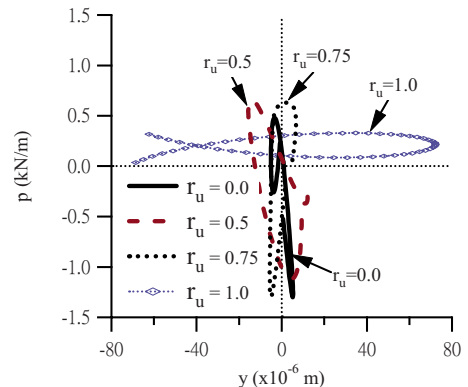


FIG. 12—Evolution of dynamic p - y response of pile A at 1.5 m deep.

shear waves are assumed. The performed test is applicable to sloping bedrock or inclined incident waves. However, as mentioned above, the kinematic and inertial effects are analyzed separately, and more insights of pile responses can be obtained.

When applying the model test results on the responses of a real pile-supported wharf, a similitude law is required to correlate the geometric and physical properties between the model and prototype. Iai (1989) derived the theoretical similitude law for 1 g shaking table model tests by considering the basic equations that governed the behaviors of the saturated soil-structure-fluid system subjected to dynamic loading and stated that the similitude law is appropriate to describe the deformation associated responses. For a 1 g model that is only $1/n$ of the prototype, the corresponding scaling factors between the prototype and model for induced strain, pore pressure, flexural rigidity (EI), bending moment (M), subgrade reaction (p), horizontal displacement (y), and acceleration are \sqrt{n} , n , $n^{3.5}$, n^3 , $n^{2.5}$, $n^{1.5}$, and 1, respectively. Accordingly, the prototype should induce \sqrt{n} times of shear strain and generate n times of Δu , but the r_u is the same. The pile responses can be evaluated from the scaling factors, and different p - y curves should exist in the projected prototype.

In summary, the performed test has the following advantages. First, it can be performed in the field to evaluate seismic resistance of active wharf and to periodically check the integrity of in situ monitoring system. Second, the instrumentation configuration and data reduction procedure can be compared to real earthquake loading in terms of soil responses and soil-structure interactions. Third, the processed shear strains are directly related to engineering properties and rigorous in mechanics aspects. Finally, the pile responses due to kinematic and inertial effects can be studied in one testing configuration. The shortcomings include less screening effect in real seismic loadings, more sensors required for strain calculation, more complicated wave field than shaking table tests and real earthquake loadings, and scale and boundary effects on state of stress and wave fields that encounter in all model tests. Although the scale effects of the performed test need further investigations, however the effects exist in all 1 g physical modeling, and the dimensions of the performed model are within the range of conventional 1 g shaking table tests reported on the literature. Nevertheless, the proposed tests can be an alternative to current large-scale physical modeling, and useful insights of soil-structure interaction can be obtained as seen in Figs. 11 and 12.

Conclusion

Field large-scale physical modeling using surface wave generator was performed to study dynamic soil-structure interactions in pile-supported wharf, verify configuration of an in situ monitoring station, and develop the technique for periodically checking of in situ instrumentation. Coupled shear strain-pore pressure generation behavior, pile responses, and soil-pile interaction characteristics were evaluated. Conclusions from preliminary results are drawn in what follows:

- (1) The testing results prove that the testing configuration and data reduction procedure can capture the interactions among the induced shear strain, generated excess pore pressure, and dynamic p - y behavior around piles.
- (2) Spatial variations of pore pressure histories show that the accumulation of excess pore pressure was affected by induced shear strain levels, pore pressure variations of nearby

soil, and distance to the pile. The rate of excess pore pressure accumulation decreases as the distance to the pile increases.

- (3) The screening effect of horizontal stress waves not only affected the induced shear strain levels ahead and behind the pile but also created different loading mechanisms for the second pile. The first pile was mainly subjected to kinematic forces from stress wave traveling through the soil, and the second pile was subjected to inertial forces from forced displacement on pile head.
- (4) The dynamic p - y curves varies with variation of excess pore pressure of surrounding soil, which is the outcome of soil stiffness reduction and change of soil impedance on wave propagation. The testing results reveal that the dynamic p - y concept should be modified for soil with significant excess pore pressure generation.

Acknowledgments

This study was supported by Harbor and Marine Technology Center, Institute of Transportation (IHMT), Taiwan, ROC, under Contract No. MOTC-IOT-96-H1DB005. This support is gratefully acknowledged. The vibroseis was provided by CPC Corporation, Taiwan. Any opinions, findings, and conclusions or recommendations expressed in this material are those of the writers and do not necessarily reflect the views of the Institute of Transportation.

References

- Boulanger, R. W., Curras, C. J., Kutter, B. L., Wilson, D. W., and Abghari, A., 1999, "Seismic Soil-Pile-Structure Interaction Experiments and Analyses," *J. Geotech. Geoenviron. Eng.*, Vol. 125, No. 9, pp. 750–759.
- Brandenberg, S. J., Boulanger, R. W., Kutter, B. L., and Chang, D., 2005, "Behavior of Pile Foundations in Laterally Spreading Ground During Centrifuge Tests," *J. Geotech. Geoenviron. Eng.*, Vol. 131, No. 11, pp. 1378–1391.
- Chang, W. J., 2002, "Development of an In Situ Dynamic Liquefaction Test," Ph.D. dissertation, University of Texas at Austin, Austin, TX.
- Cubrinovski, M., Kokusho, T., and Ishihara, K., 2006, "Interpretation from Large-Scale Shake Table Tests on Piles Undergoing Lateral Spreading in Liquefied Soils," *J. Soil Dyn. Earthquake Eng.*, Vol. 26, No. 2–4, pp. 275–286.
- Dou, H. and Byrne, P. M., 1996, "Dynamic Response of Single Piles and Soil-Pile Interaction," *Can. Geotech. J.*, Vol. 33, pp. 80–96.
- Dunnivant, T. W. and O'Neill, M. W., 1989, "Experimental p - y Model for Submerged, Stiff Clay," *J. Geotech. Eng.*, Vol. 115, No. 1, pp. 95–114.
- Iai, S., 1989, "Similitude for Shaking Table Tests on Soil-Structure-Fluid Model in 1g Gravitational Field," *Soils Found.*, Vol. 29, No. 1, pp. 105–118.
- Kamijo, N., Saito, H., Kusama, K., Kontani, O., and Nigbor, R., 2004, "Seismic Tests of a Pile-Supported Structure in Liquefiable Sand Using Large-Scale Blast Excitation," *Nucl. Eng. Des.*, Vol. 228, pp. 367–376.
- Klar, A. and Frydman, S., 2002, "Three-Dimensional Analysis of Lateral Pile Response Using Two-Dimensional Explicit Nu-

- merical Scheme," *J. Geotech. Geoenviron. Eng.*, Vol. 128, No. 9, pp. 775–784.
- Mondal, G. and Rai, D. C., 2008, "Performance of Harbour Structures in Andaman Islands During 2004 Sumatra Earthquake," *Eng. Struct.*, Vol. 30, No. 1, pp. 174–182.
- Nakamura, S., 1995, *Applied Numerical Method in C*, Prentice Hall, Englewood Cliffs, NJ.
- Rathje, E. M., Chang, W. J., and Stokoe, K. H. II, 2005, "Development of an In Situ Dynamic Liquefaction Test," *Geotech. Test. J.*, Vol. 28, No. 1, pp. 50–60.
- Rollins, K. M., Gerber, T. M., Lane, J. D., and Asford, S. A., 2005, "Lateral Resistance of a Full-Scale Pile Group in Liquefied Sand," *J. Geotech. Geoenviron. Eng.*, Vol. 131, No. 1, pp. 115–125.
- Rollins, K. M. and Sparks, A., 2002, "Lateral Resistance of Full-Scale Pile Cap with Gravel Backfill," *J. Geotech. Geoenviron. Eng.*, Vol. 128, No. 9, pp. 711–23.
- Takahashi, A. and Takemura, J., 2005, "Liquefaction-Induced Large Displacement of Pile-Supported Wharf," *Soil. Dyn. Earthquake Eng.*, Vol. 25, No. 11, pp. 811–825.
- Tokimatsu, K. and Asaka, Y., 1998, "Effects of Liquefaction-Induced Ground Displacements on Pile Performance in the 1995 Hyogoken-Nambu Earthquake," *Spec Issue Soils Found.*, Vol. 2, pp. 163–77.
- Tokimatsu, K. and Suzuki, H., 2004, "Pore Water Pressure Response Around Pile and Its Effects on p - y Behavior During Soil Liquefaction," *Soils Found.*, Vol. 44, No. 6, pp. 101–110.
- Wang, S. T. and Reese, L. C., 1998, "Design of Pile Foundations in Liquefied Soils," *Geotechnical Earthquake Engineering and Soil Dynamics III, GSP No. 75*, Vol. 2, P. Dakoulas and M. Yegian, Eds., ASCE, Reston, VA, pp. 1331–1343.
- Werner, S. D., Dickenson, S. E., Egan, J. A., Ferritto, J. M., Kaldveer, P., Thiessen, D. A., Serventi, G. M., and Byrne, E. F., 1998, "Chapter 2: Experience from Past Earthquakes," *Seismic Guidelines for Ports, TCLEE, Monograph No. 12*, S. D. Werner, Ed., ASCE, Reston, VA.
- Woods, R. D., 1968, "Screening of Surface Waves in Soils," *J. Soil Mech. and Found. Div.*, Vol. 94, No. SM4, pp. 951–979.